

Graphene-incorporated chitosan substrata for adhesion and differentiation of human mesenchymal stem cells†

Cite this: *J. Mater. Chem. B*, 2013, **1**, 933Received 18th October 2012
Accepted 2nd January 2013

DOI: 10.1039/c2tb00274d

www.rsc.org/MaterialsB

Jangho Kim,^{‡a} Yang-Rae Kim,^{‡b} Yeonju Kim,^c Ki Taek Lim,^a Hoon Seonwoo,^a Subeom Park,^b Sung-Pyo Cho,^b Byung Hee Hong,^b Pill-Hoon Choung,^d Taek Dong Chung,^{*b} Yun-Hoon Choung^{*c} and Jong Hoon Chung^{*ae}

A simple method that uses graphene to fabricate nanotopographic substrata was reported for stem cell engineering. Graphene-incorporated chitosan substrata promoted adhesion and differentiation of human mesenchymal stem cells (hMSCs). In addition, we proposed that nanotopographic cues of the substrata could enhance cell–cell and cell–material interactions for promoting functions of hMSCs.

Stem cells are characterized by their unique ability to differentiate into various types of cells, yielding an important key in regenerative medicine.¹ Stem cells can display high sensitivity to the nanoscale topography of the extracellular matrix.¹ It is therefore important to develop a platform for regulating or improving stem cell functions from an integrative aspect of biology and engineering.¹ Recently, graphene, a new carbon-based nanomaterial, has emerged as a pronounced potential for stem cell and tissue engineering applications due to its unique physicochemical properties including nanotopography as well as good biocompatibility.² For example, Nayak *et al.* reported that graphene-coated substrata accelerated osteogenesis of human mesenchymal stem cells (hMSCs).^{2d}

Here, we develop a simple method for fabrication of graphene-based nanotopographic substrata for stem cell engineering. We hypothesize that the graphene-based substrata can feature as unique nanotopography and provide effective

environments to promote functions of stem cells. To address this challenge, we fabricated graphene-incorporated chitosan substrata and investigated whether they would promote functions of stem cells. In this study, we cultured hMSCs on the graphene-incorporated chitosan substrata and found that nanotopographic cues of the substrata promoted adhesion and differentiation of hMSCs. This reveals an insight for design and fabrication of scaffolds, which can be used for stem cell-based tissue engineering and regenerative medicine.

Fig. 1A shows a schematic illustration of the preparation of nanotopography platforms using graphene and chitosan. Reduced graphene oxide (RGO)–chitosan substrata were fabricated after spin-coating of the RGO–chitosan composites (Fig. 1B) on bare glass. It is noted that RGO was well dispersed in chitosan solution (Fig. 1B). We observed that the RGO–chitosan substrata featured transparent properties (Fig. 1B and S1†) and nanodot-like nanotopography (Fig. 1C). Various layers of RGO were occasionally observed in the RGO–chitosan nanocomposite. However, RGO was homogeneously distributed through spin-coating in the RGO–chitosan nanocomposite. Therefore, nanotopography by incorporation of RGO can induce variation of surface roughness at the nanoscale level. As a result, it may be able to influence the growth and differentiation of stem cells.

To confirm this assumption, we investigated the surface coverage and roughness in the RGO–chitosan nanocomposites. The surface coverage values of RGO (surface area of RGO to whole RGO–chitosan ratio), as measured with ImageJ software, with 0.05, 0.5, and 5% w/w RGO compositions were 0.009, 0.014, and 0.049, respectively (Fig. S2†). The average surface roughness values of RGO–chitosan substrata with 0, 0.05, 0.5, and 5% w/w RGO compositions, as measured by atomic force microscope (AFM) imaging, were estimated to be 0.9, 1.5, 3.7, and 7.7 nm, respectively (Fig. S3†). We also observed that the incorporation of graphene into the chitosan substrata slightly increased the hydrophobic properties of the chitosan substrata (Fig. S4†).

In addition, we confirmed that the Raman spectrum of RGO–chitosan substrata had two broad peaks, which are

^aDepartment of Biosystems & Biomaterials Science and Engineering, Seoul National University, Seoul 151-742, Republic of Korea. E-mail: jchung@snu.ac.kr

^bDepartment of Chemistry, Seoul National University, Seoul 151-747, Republic of Korea. E-mail: tdchung@snu.ac.kr

^cDepartment of Otolaryngology, Ajou University School of Medicine, Suwon 443-721, Republic of Korea. E-mail: yhc@ajou.ac.kr

^dDepartment of Oral and Maxillofacial Surgery, School of Dentistry, Seoul National University, Seoul, Republic of Korea

^eResearch Institute for Agriculture and Life Sciences, Seoul National University, Seoul 151-742, Republic of Korea

† Electronic supplementary information (ESI) available. See DOI: 10.1039/c2tb00274d

‡ These authors contributed equally to this work.

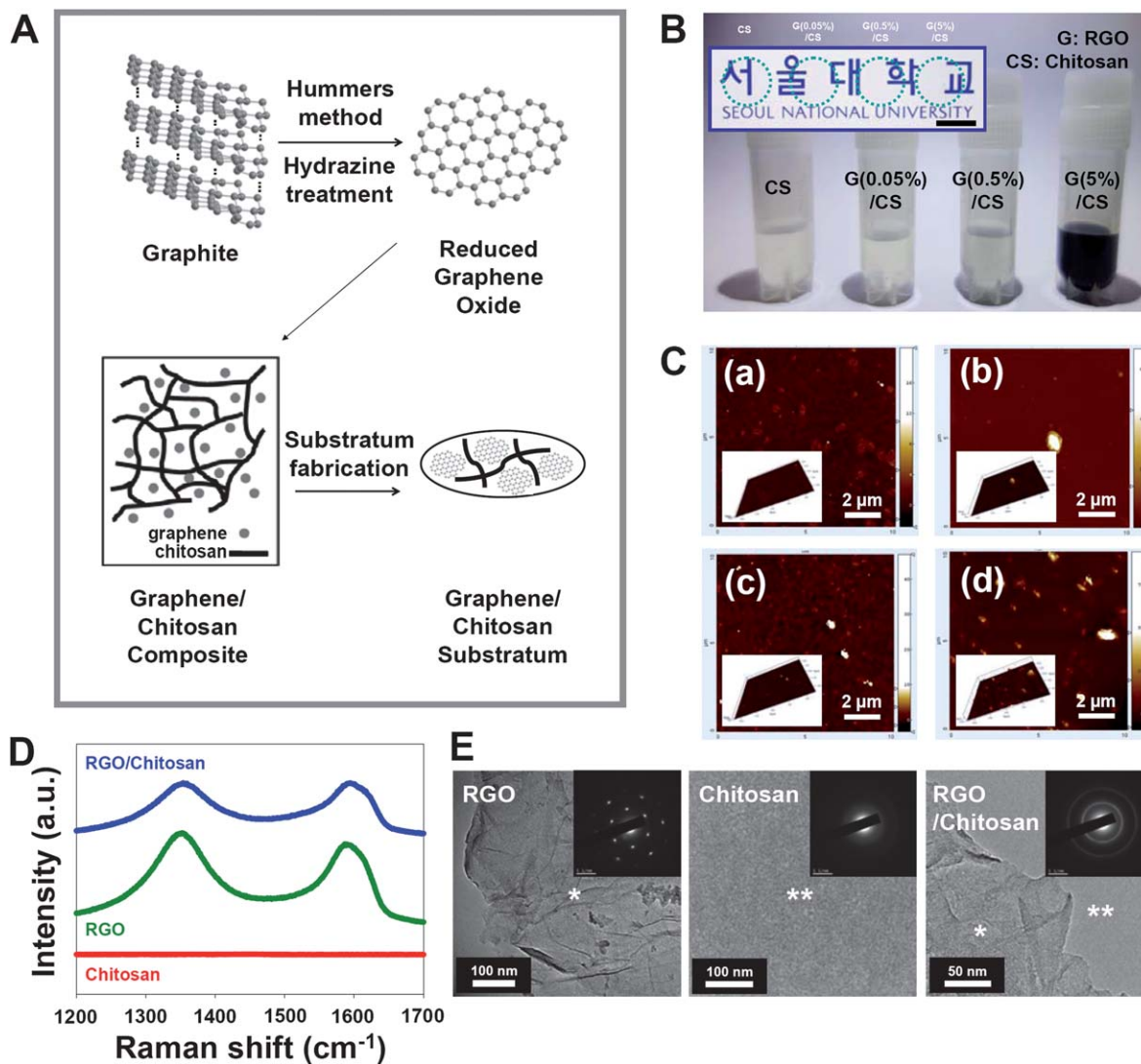


Fig. 1 (A) Schematic illustration showing the synthesis of graphene-incorporated chitosan nanocomposite substrata. (B) Photograph of chitosan solution and RGO–chitosan composite solutions. The inset shows a photograph of the transferred chitosan substratum and RGO–chitosan substrata, the dot-circles indicate the substrata, and the scale bar represents 1 mm. (C) AFM images of RGO–chitosan substrata of the following compositions: (a) 0, (b) 0.05, (c) 0.5, and (d) 5% (w/w) RGO. (D) Raman spectra of RGO sheets, chitosan, and 5% RGO–chitosan substratum. (E) TEM images of RGO sheets, chitosan, and 5% RGO–chitosan substratum. The (*) and (**) indicate RGO and chitosan, respectively. Insets are the corresponding SAED patterns.

known as the G and D bands ($\sim 1590\text{ cm}^{-1}$ and $\sim 1350\text{ cm}^{-1}$ respectively) (Fig. 1D). Fig. 1E shows representative transmission electron microscopy (TEM) images and the corresponding selected area electron diffraction (SAED) patterns (inset) of a RGO sheet, chitosan, and 5% RGO–chitosan substratum, respectively. We observed that the sizes of RGO sheets ranged from 0.5 to 2 μm (Fig. 1E and S5A[†]). A typical SAED pattern obtained from a RGO sheet shows the six-fold symmetry expected for graphite or graphene (Fig. 1E). It is confirmed that the synthesized RGO sheets are monolayer graphene from the analysis of the intensity ratio of the diffraction peaks, an inner hexagon (01 $\bar{1}$ 0) and an outer hexagon (11 $\bar{2}$ 0).^{2g,h} This result is consistent with the previous Raman result (Fig. 1D). Also, the hollow ring patterns that are characteristic of an amorphous phase were observed on the

chitosan substratum. Furthermore, a typical SAED pattern forms a circle in the RGO–chitosan substratum, which displayed continuous and broad ring patterns. The two diffraction rings correspond to graphene crystal planes: an inner ring (01 $\bar{1}$ 0) corresponding to a lattice spacing of 0.213 nm and an outer ring (11 $\bar{2}$ 0) corresponding to a lattice spacing of 0.123 nm (Fig. 1E and S5[†]). This indicated that the monolayer RGO sheets were well dispersed with small domain sizes on the chitosan substratum. In order to confirm the above results for the RGO–chitosan substratum, a high-resolution TEM (HRTEM) study was carried out. Fig. S5B[†] shows a magnified HRTEM image of an edge area of the RGO–chitosan substratum shown in Fig. 1E. We also observed some randomly distributed small crystalline regions (marked by the dotted red circles), and the sizes of these small domains were

within the range of 3–10 nm (Fig. S5†). The parallel fringes corresponding to 4–5 graphene layers at the edge area and wrinkles within the substrata were visible. These results indicate that the graphene-incorporated chitosan substrata were successfully fabricated with nanotopography.

To verify the hypothesis that the nanotopography of RGO–chitosan substrata can provide effective environments to promote functions of stem cells, we first observed the adhesion of hMSCs on RGO–chitosan substrata (Fig. S6†). We cultured hMSCs on the RGO–chitosan substrata, chitosan substrata, and tissue culture polystyrene (TCPS) as controls. At 6 h after cell seeding, we carefully removed unattached hMSCs from the substrata and TCPS by washing with phosphate buffered saline to check the attachment of hMSCs onto the sample surface. Viability measurements for hMSC growth on RGO–chitosan substrata, chitosan substrata, and TCPS are shown in Fig. S6†, which indicate that RGO–chitosan substrata, regardless of the incorporated graphene concentration, provided a suitable environment for hMSC adhesion. Interestingly, we found that hMSC adhesion was greater on the 5% RGO–chitosan substrata than on other samples, with the exception of TCPS, although no significant differences were observed statistically ($P > 0.05$). We also showed in this finding that the hMSCs on the 5% RGO–chitosan substratum were more attached than those on the chitosan substratum by the phase contrast micrographs (Fig. S7†).

The proliferation of hMSCs on RGO–chitosan substrata was continually observed and quantified at 1, 3, and 5 days. All samples including the RGO–chitosan substrata, regardless of the incorporated graphene concentration, showed time-dependent proliferation of hMSCs after adhering to the sample surface at 6 h (Fig. S8A†). To confirm the growth of hMSCs on RGO–chitosan substrata, we examined the cells under a FESEM after 5 days of hMSC culture. Fig. S8B(b)† shows that hMSCs were adhered and spread properly on almost the entire surface of the 5% RGO–chitosan substrata, and similar observation of the hMSCs cultured on chitosan-only substrata (Fig. S8B(a)†), indicating that the RGO–chitosan substrata might provide a suitable environment for the proliferation of hMSCs.

We observed that the proliferation rate of hMSCs decreased with incorporation of higher amounts of graphene into the substrata (Fig. S8A†). The following two possibilities may be responsible for the above finding: (1) graphene is cytotoxic or (2) hMSCs differentiate into other lineages because of the unique properties of the graphene incorporated into the substrata including nanotopography. Recent studies reported that graphene or graphene oxide (GO) was cytotoxic at concentrations greater than $50 \mu\text{g mL}^{-1}$.³ On the other hand, we analyzed the cytotoxicity of GO in hMSCs, and found that low concentrations (less than 0.1 mg mL^{-1}) of GO did not show cytotoxicity in hMSCs, while high concentrations (greater than 0.1 mg mL^{-1}) were somewhat cytotoxic to hMSCs (Fig. S9†). We used very less amount of RGO for fabrication of substrata (e.g., very little RGO–chitosan composite solution less than $100 \mu\text{L}$ of 0.01 mg mL^{-1} RGO solution was used to fabricate the 0.05% RGO–chitosan substrata), which indicated

that the cytotoxicity of graphene might not be the main reason for the lower proliferation rate of hMSCs on RGO–chitosan substrata than on chitosan substrata or TCPS. However, additional investigations are required to further analyze the cytotoxicity of graphene to hMSCs. Thus, we noted the second possibility of the low proliferation rates of hMSCs on the RGO–chitosan substrata that the incorporated graphene into the substrata might positively influence differentiation of hMSCs. This finding is consistent with that reported in a recent study that graphene accelerated osteogenic differentiation of hMSCs, although graphene films were used as stem cell culture platforms.^{2e}

To verify this hypothesis that graphene in chitosan substrata enhances the differentiation of hMSCs, we first checked the osteogenesis of hMSCs on RGO–chitosan substrata. We cultured hMSCs on the RGO–chitosan substrata and also on the chitosan substrata and TCPS as controls with or without differentiation-inducing chemicals. After 21 days of hMSC culture on the sample surfaces, we analyzed hMSC osteogenesis by Alizarin Red S staining. To quantify the degree of osteogenesis, the stained calcium deposits were destained with cetylpyridinium chloride, and then the extracted stains were measured using an ELISA reader. As shown in Fig. 2A, we showed our observation with significantly higher values, absorbance at 540 nm, for hMSC cultured on the RGO–chitosan substrata compared to that on the chitosan substrata and TCPS both in the normal and osteogenic induction media ($P < 0.05$). Interestingly, the 5% RGO–chitosan substrata exhibited the highest osteogenesis ($P < 0.01$). We further examined osteocalcin (OCN) as one of the osteogenic genes to confirm enhanced osteogenic differentiation of hMSCs on the 5% RGO–chitosan substrata. Western blot analysis clearly showed up-regulation of the OCN protein in the graphene–chitosan substrata compared to the chitosan substrata and TCPS both in the normal and osteogenic induction media (Fig. 2B). Since expression of OPN is often co-localized with members of the matrix metalloproteinase (MMP) family and it has been known that MMP-cleaved OPN plays an important role in increasing the activity of cell adhesion and functions,⁴ we also checked protein expression of the MMP-cleaved OPN of hMSCs on the samples. Interestingly, the results of western blot analysis showed more protein expression of the MMP-cleaved OPN on the 5% RGO–chitosan substrata compared to the chitosan substrata and TCPS both in the normal and osteogenic induction media (Fig. 2B), suggesting that the enhanced MMP-cleaved OPN of hMSCs on the RGO–chitosan substrata might increase the activity in promoting hMSC adhesion as well as functions including osteogenesis. Together, these findings suggest that graphene incorporated into chitosan substrata can promote the osteogenesis of hMSCs despite the small amount of graphene used.

We then checked the neurogenesis of hMSCs on the 5% RGO–chitosan substrata since we expected that their nanotopography as well as electronic properties of the graphene in the substrata would have great potential as a stem cell culture to differentiate stem cells into electrically exciting cells. To investigate the effect of RGO–chitosan substrata on neurogenesis of

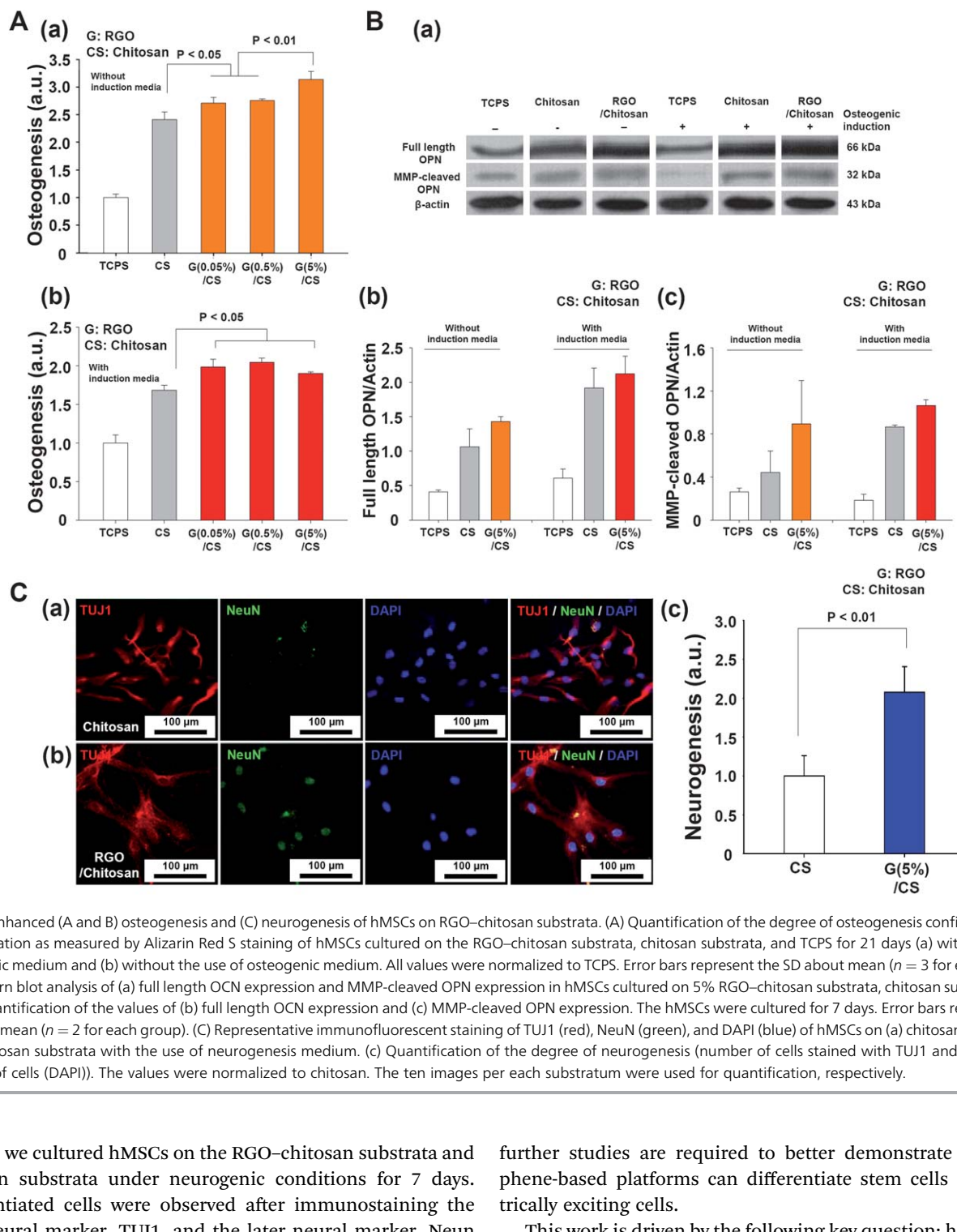


Fig. 2 Enhanced (A and B) osteogenesis and (C) neurogenesis of hMSCs on RGO–chitosan substrata. (A) Quantification of the degree of osteogenesis confirmed by the mineralization as measured by Alizarin Red S staining of hMSCs cultured on the RGO–chitosan substrata, chitosan substrata, and TCPS for 21 days (a) with the use of osteogenic medium and (b) without the use of osteogenic medium. All values were normalized to TCPS. Error bars represent the SD about mean ($n = 3$ for each group). (B) Western blot analysis of (a) full length OCN expression and MMP-cleaved OPN expression in hMSCs cultured on 5% RGO–chitosan substrata, chitosan substrata, and TCPS. Quantification of the values of (b) full length OCN expression and (c) MMP-cleaved OPN expression. The hMSCs were cultured for 7 days. Error bars represent the SD about mean ($n = 2$ for each group). (C) Representative immunofluorescent staining of TUJ1 (red), NeuN (green), and DAPI (blue) of hMSCs on (a) chitosan and (b) 5% RGO–chitosan substrata with the use of neurogenesis medium. (c) Quantification of the degree of neurogenesis (number of cells stained with TUJ1 and NeuN/total number of cells (DAPI)). The values were normalized to chitosan. The ten images per each substratum were used for quantification, respectively.

hMSCs, we cultured hMSCs on the RGO–chitosan substrata and chitosan substrata under neurogenic conditions for 7 days. Differentiated cells were observed after immunostaining the early neural marker, TUJ1, and the later neural marker, NeuN (Fig. 2C). We observed that the differentiated cells had neuron-like morphology on both the samples. We found a more adhered shape of differentiated cells on the RGO–chitosan substrata compared to those on the chitosan substrata. Interestingly, as shown in Fig. 2C, we learned that most of the later neural markers were stained by culturing hMSCs on the RGO–chitosan substrata whereas the markers were a little stained on the chitosan substrata. Our findings suggest that RGO–chitosan substrata may promote the neurogenesis of hMSCs although

further studies are required to better demonstrate that graphene-based platforms can differentiate stem cells into electrically exciting cells.

This work is driven by the following key question: how do the graphene-incorporated chitosan nanocomposite substrata enhance the differentiation of hMSCs? Although detailed basic research on this issue remains to be performed including specific signaling pathway, we hypothesize that the unique characteristics of the nanoscale topographical cue of graphene and its secondary effects such as stiffness and roughness within substrata might play a crucial role in the enhancement of hMSC differentiation. Recently, it has been generally accepted that the differentiation of hMSCs is controlled by nanostructures. In

particular, Dalby and colleagues have reported that the nanoscale disorder of substrates can stimulate the osteogenesis of hMSCs, whereas the nanoscale symmetry of substrates allows for the maintenance of hMSC multipotency.⁵ In our RGO–chitosan substrata, graphene was incorporated asymmetrically into the chitosan substrata, and their nanostructures were maintained (Fig. 1C). Hence, the nanoscale disorder of graphene incorporated into the chitosan substrata might enhance hMSC osteogenesis. Moreover, the nanoscale symmetry of graphene incorporated into the chitosan substrata may be another important issue in the potential application of graphene as substrata for hMSCs.

It is widely accepted that enhanced cell spreading and interaction between cell–substrate or cell–cell are important factors to be considered for enhancing differentiation of hMSCs.⁶ As we confirmed the enhanced MMP-cleaved OPN in hMSCs on the RGO–chitosan substrata compared to those on the chitosan substrata, we speculated that the incorporated graphene in chitosan substrata could influence initial cell adhesion and interaction between cell–cell or cell–substrate, which might be another possible explanation to enhance the differentiation of hMSCs on the RGO–chitosan substrata.

To investigate whether the incorporated graphene in chitosan substrata influenced the initial behavior of hMSCs, we cultured hMSCs on the RGO–chitosan substrata and chitosan substrata for 3 days in the normal media. More spread shape of hMSCs on the RGO–chitosan substrata was observed in immunohistochemical analysis compared to that on the chitosan substrata (Fig. 3A). We also observed that the incorporated graphene in chitosan substrata greatly influenced the focal adhesions (FAs) of the hMSCs. The hMSCs on the RGO–chitosan substrata showed a large number of FAs, as obtained by vinculin immunostaining, than on the chitosan substrata (Fig. 3B). Furthermore, western blot analysis clearly showed greatly enhanced expression of the integrin $\beta 1$ in cultured hMSCs on the RGO–chitosan substrata compared to that on the chitosan substrata (Fig. 3C). It is noted that OPN increases integrin $\beta 1$ expression in MSCs.⁷ These findings especially show that the hMSCs may have a higher cell–substrate interaction in RGO–chitosan substrata compared to chitosan substrata. In addition, we observed that the graphene in RGO–chitosan substrata greatly influence cell–cell contacts (Fig. 3A). Furthermore, western blot analysis clearly showed enhanced expression of the major junction protein connexin 43 (Cx43) in

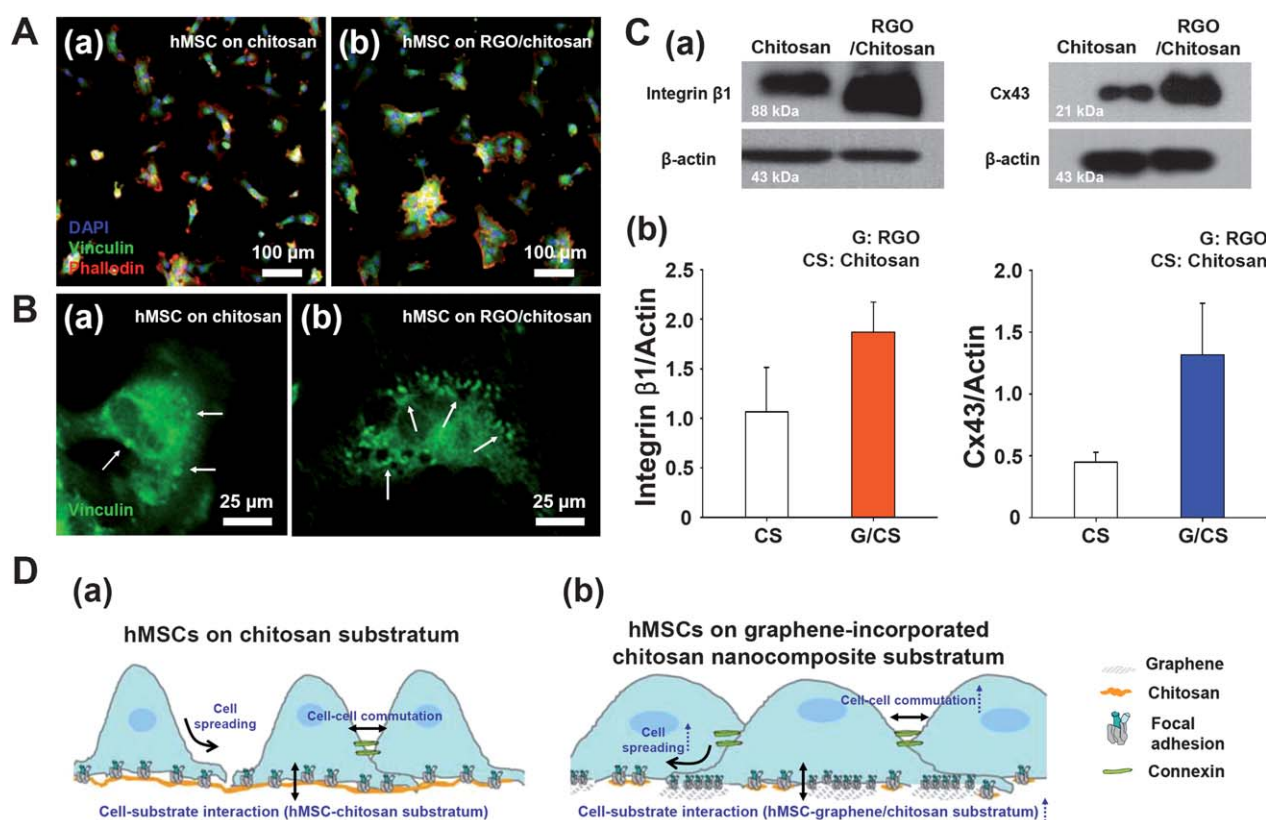


Fig. 3 Model for the enhanced differentiation of hMSCs on RGO–chitosan substrata through increased initial cell adhesion, cell–substrate interaction, and cell–cell contacts by the nanoscale topographical cues of graphene within chitosan substrata. (A) Representative immunofluorescent images with low magnification of the adhered hMSCs on chitosan and 5% RGO–chitosan substrata. (B) Representative immunofluorescent images with high magnification of adhered hMSCs on chitosan and 5% RGO–chitosan substrata. The white arrows indicate focal adhesion (FA) of adhered hMSCs on the substrata. The hMSCs were cultured for 3 days. (C) Western blot analysis and quantification of the values of integrin $\beta 1$ and Cx43 expression of hMSCs cultured on chitosan and 5% RGO–chitosan substrata. The hMSCs were cultured for 3 days. Error bars represent the SD about mean ($n = 2$ for each group). (D) A hypothetical model showing the enhanced initial cell adhesion (spreading hMSCs), cell–cell contacts (FAs and integrin $\beta 1$), and cell–substrate interaction (Cx43) on the 5% RGO–chitosan substrata to support further differentiation of hMSCs. All figures are magnified for clarity.

cultured hMSCs on the RGO–chitosan substrata compared to that on the chitosan substrata (Fig. 3C).

Together, these findings indicate that the incorporated graphene in chitosan substrata provides specific cues to hMSCs, resulting in enhanced cell–cell communication. Our results suggest that the graphene with unique characteristics of the nanoscale topographical cue within chitosan substrata and its secondary effects such as stiffness and roughness may promote the differentiation of hMSCs. Simply, the proposed mechanism follows these steps: graphene cues in substrate → enhancing hMSCs spreading on substrata and interactions between hMSC–substrate and hMSC–hMSC → enhancing differentiation of hMSCs (see Fig. 3D for a summary of this possible mechanism). In addition, a recent study reported that graphene might allow accelerated differentiation of hMSCs through strong noncovalent binding abilities for molecular interactions.^{2e}

We would like to re-emphasize our findings that the graphene nanosheets were well dispersed in the RGO–chitosan substrata (Fig. 1E and S5[†]) and they could significantly enhance the adhesion and differentiation of hMSCs even without requiring the use of any differentiation-inducing chemicals in the case of osteogenesis (Fig. 2). Namely, we showed a potential that a small amount of graphene in polymer-based substrata could improve functions of stem cells.

We believe that this study may represent a significant progression in the clinical application of stem cell-based tissue engineering. For example, this simple method, incorporating small amounts of graphene into scaffolds, may be a powerful strategy for the design and manipulation of nanotopographies as a potential scaffold in the fields of stem cell and tissue engineering, including bone and nerve regeneration. While we have used chitosan for fabrication of graphene-incorporated substrata in the present study, our method is expected to be applicable to other polymers such as gelatin, polycaprolactone, poly(D,L-lactide-co-glycolide), etc. Our method may also allow the fabrication of a graphene-based three-dimensional scaffold using a combination of convenient scaffold fabrication methods such as freezing and lyophilizing, thermally induced phase separation, porogen leaching, gas foaming, or electrospinning.

In summary, we have demonstrated that graphene-incorporated chitosan nanocomposites can be used to enhance the adhesion and differentiation of hMSCs. Our results indicate that RGO–chitosan substrata with asymmetrical nanotopology provided a suitable environment for the adhesion and proliferation of hMSCs as well as enhanced cell–substrate interaction and cell–cell contacts. The RGO–chitosan substrata promoted the osteogenesis of hMSCs both in the absence and presence of differentiation-inducing chemicals. The RGO–chitosan substrata also enhanced the neurogenesis of hMSCs. Our work implies that the methodology for the fabrication of graphene-incorporated chitosan nanocomposites can be adapted for the design and manipulation of other scaffolds with nanotopography. We conclude that graphene-incorporated chitosan substrata can be used as an efficient strategy for stem cell and potential tissue engineering applications.

Acknowledgements

This work was supported by the National Research Foundation of Korea (NRF) grant funded by the Korea government (2012R1A1A2009165), the Korea Health 21 R&D Project, Ministry of Health & Welfare, Republic of Korea (A120485), and the Industrial Source Technology Development Program (10033657) of the Ministry of Knowledge Economy (MKE) of Korea. Y.-R. Kim was supported by the Brain Korea 21 fellowship.

Notes and references

- (a) M. P. Lutolf and H. M. Blau, *Adv. Mater.*, 2009, **21**, 3255; (b) F. Guilak, D. M. Cohen, B. T. Estes, J. M. Gimble, W. Liedtke and C. S. Chen, *Cell Stem Cell*, 2009, **5**, 17; (c) J. Kim, C. Cho, Y. Choung, K. Lim, H. Son, H. Seonwoo, S. Baik, S. Jeon, J. Park, P. Choung and J. Chung, *Tissue Eng. Regener. Med.*, 2009, **6**, 199; (d) J. Kim, D. Kim, K. Lim, H. Seonwoo, S. Park, Y. Kim, Y.-R. Kim, Y. Choung, P. Choung and J. Chung, *Tissue Eng., Part C*, 2012, **18**, 913; (e) N. Naveena, J. Venugopal, R. Rajeswari, S. Sundarajan, R. Sridhar, M. Shayanti, S. Narayanan and S. Ramakrishna, *J. Mater. Chem.*, 2012, **22**, 5239; (f) J. T. Koepsel, P. T. Brown, S. G. Loveland, W.-J. Li and W. L. Murphy, *J. Mater. Chem.*, 2012, **22**, 19474.
- (a) D. A. Stout and T. J. Webster, *Mater. Today*, 2012, **15**, 312; (b) C. Zhao, A. Tan, G. Pastorin and H. K. Ho, *Biotechnol. Adv.*, 2012, DOI: org/10.1016/j.biotechadv.2012.08.001; (c) Y.-R. Kim, S. Bong, Y.-J. Kang, Y. Yang, R. K. Mahajan, J. S. Kim and H. Kim, *Biosens. Bioelectron.*, 2010, **25**, 2366; (d) T. R. Nayak, H. Andersen, V. S. Makam, C. Khaw, S. Bae, X. Xu, P. R. Ee, J.-H. Ahn, B. H. Hong, G. Pastorin and B. Ozyilmaz, *ACS Nano*, 2011, **5**, 4670; (e) W. C. Lee, C. H. Y. X. Lim, H. Shi, L. A. L. Tang, Y. Wang, C. T. Lim and K. P. Loh, *ACS Nano*, 2011, **5**, 7334; (f) J. Liu, J. Tang and J. J. Gooding, *J. Mater. Chem.*, 2012, **22**, 12435; (g) S. Horischi, T. Gotou and M. Fujiwara, *Appl. Phys. Lett.*, 2004, **84**, 2403; (h) A. C. Ferrari, J. C. Meyer, V. Scardaci, C. Casiraghi, M. Lazzeri, F. Mauri, S. Piscanec, D. Jiang, K. S. Novoselov, S. Roth and A. K. Geim, *Phys. Rev.*, 2006, **97**, 187401.
- (a) K. Wang, J. Ruan, H. Song, J. Zhang, Y. Wo, S. Guo and D. Cui, *Nanoscale Res. Lett.*, 2011, **6**, 8; (b) K. Liao, Y. Lin, C. Macosko and C. Haynes, *ACS Appl. Mater. Interfaces*, 2011, **3**, 2607.
- R. Agnihotri, H. C. Crawford, H. Haro, L. M. Matrisian, M. C. Havrda and L. Liaw, *J. Biol. Chem.*, 2001, **276**, 28261.
- (a) M. J. Dalby, N. Gadegaard, R. Tare, A. Andar, M. O. Riehle, P. Herzyk, C. D. W. Wilkinson and R. O. C. Oreffo, *Nat. Mater.*, 2007, **6**, 997; (b) R. J. McMurray, N. Gadegaard, P. M. Tsimbouri, K. V. Burgess, L. E. McNamara, R. Tare, K. Murawski, E. Kingham, R. O. C. Oreffo and M. J. Dalby, *Nat. Mater.*, 2011, **10**, 637.
- (a) R. McBeath, D. M. Pirone, C. M. Nelson, K. Bhadriraju and C. S. Chen, *Dev. Cell*, 2004, **6**, 483; (b) K. A. Killian, B. Bugarija, B. T. Lahn and M. Mrksich, *Proc. Natl. Acad. Sci. USA*, 2010, **107**, 4872; (c) J. Tang, R. Peng and J. Ding, *Biomaterials*, 2010, **31**, 2470.
- C. Zou, G. Song, G. Luo, L. Yuan and L. Yang, *In Vitro Cell. Dev. Biol.: Anim.*, 2011, **47**, 241.